16

Vibration Reduction via the Boundary Control Method

Siddharth P. Nagarkatti
Lucent Technologies

Darren M. Dawson
Clemson University

16.1 Introduction

The dynamics of flexible mechanical systems that require vibration reduction are usually mathematically represented by partial differential equations (PDEs). Specifically, flexible systems are modeled by a PDE that is satisfied over all points within a domain and a set of boundary conditions. These static or dynamic boundary conditions must be satisfied at the points bounding the domain. Traditionally, PDE-based models for flexible systems have been discretized via modal analysis in order to facilitate the control design process. One of the disadvantages of using a discretized model for control design is that the controller could potentially excite the unmodeled, high-order vibration modes neglected during the discretization process (i.e., spillover effects), and thereby, destabilize the closed-loop system. In recent years, distributed control techniques using smart sensors and actuators (e.g., smart structures) have become popular; however, distributed sensing/actuation is often either too expensive to implement or impractical. More recently, boundary controllers have been proposed for use in vibration control applications. In contrast to using the discretized model for the control design, boundary controllers are derived from a PDE-based model and thereby, avoid the harmful spillover effects. In contrast to distributed sensing/actuation control techniques, boundary controllers are applied at the boundaries of the flexible system, and as a result, require fewer sensors/actuators.

In this chapter, we introduce the reader to the concept of applying boundary controllers to mechanical systems. Specifically, we first provide a motivating example to illustrate in a heuristic manner how a boundary controller is derived via the use of a Lyapunov-like approach. To this end, we now examine the following simple flexible mechanical system* described by the PDE

*This PDE model is the so-called wave equation which is often used to model flexible systems such as cables or strings.

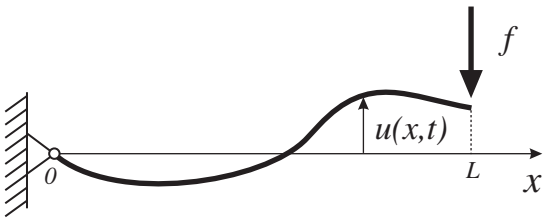

FIGURE 16.1 Schematic diagram of the string system.

$$u_{tt}(x,t) - u_{xx}(x,t) = 0 \tag{16.1}$$

along with the boundary conditions

$$u(0,t) = 0 \quad u_x(L,t) = f(t) \tag{16.2}$$

where $x \in [0, L]$ denotes the independent position variable, t denotes the independent time variable, $u(x,t)$ denotes the displacement at position x for time t, the subscripts x, t represent partial derivatives with respect to x, t, respectively, and $f(t)$ is a control input applied at the boundary position $x = L$. The flexible system described by Equations (16.1) and (16.2) can be schematically represented as shown in Figure 16.1.

The control objective involves designing the control force $f(t)$ to eliminate vibrations throughout the entire system domain using only boundary measurements. Specifically, the aim is to drive $u(x,t) \to 0 \forall x \in [0, L]$ as $t \to \infty$. The underlying philosophy of this control problem is that $f(t)$ should behave as an active *virtual damper* that sucks the energy out of the system. It should be noted that the degree of complexity of this damper-like force is often directly related to the system model. For the linear PDE model of (16.1) and (16.2), only a simple damper in the form of a negative boundary-velocity feedback term at $x = L$ is sufficient to eliminate vibrations throughout the entire system. However, as will be seen in later examples, a more sophisticated boundary control law is often required for more complicated flexible, mechanical system models.

To illustrate the boundary control design procedure, let us consider the following boundary control law for the system described by (16.1) and (16.2):

$$f(t) = -ku_t(L,t) \tag{16.3}$$

where k is a positive, scalar control gain. Note that the above controller is only dependent on measurement of the velocity $u_t(x,t)$ at the boundary position $x = L$. The structure of (16.3) is based on the concept that negative velocity feedback increases the damping in the system. A Lyapunov-like analysis method may be used to illustrate displacement regulation in the system. To this end, the following differentiable, scalar function, composed of the kinetic and potential energy, is defined as follows:

$$V(t) = \tfrac{1}{2}\int_0^L u_t^2(\sigma,t)d\sigma + \tfrac{1}{2}\int_0^L u_\sigma^2(\sigma,t)d\sigma + 2\beta\int_0^L \sigma u_t(\sigma,t)u_\sigma(\sigma,t)d\sigma \tag{16.4}$$

where β is a small, positive weighting constant that is used to ensure that $V(t)$ is non-negative. It should be noted that while the weighting constant β is used in the analysis, it does not appear in

the control law of (16.3). After some algebraic manipulation and integration by parts,* the evaluation of the time derivative of (16.4) along (16.1), (16.2), and (16.3) produces

$$\dot{V}(t) \le -\beta \int_0^L \left(u_t^2(\sigma,t) + u_\sigma^2(\sigma,t) \right) d\sigma \tag{16.5}$$

for a sufficiently small β. Upon application of some standard integral inequalities[1] to (16.4) and (16.5), it can be shown that $u(x,t) \to 0 \forall x \in [0,L]$ as $t \to \infty$; hence, the vibration along the entire domain is driven to zero. We note that the third term of (16.4) is crucial in obtaining the structure of the time derivative of the Lyapunov function given by (16.5); however, the physical interpretation for this term in the Lyapunov function is difficult to explain.

With the above simple example serving to lay the groundwork, we will now focus our attention on the discussion of more complex PDE models often used to describe specific engineering applications. That is, we first present a model-based boundary controller that regulates the out-of-plane vibration of a cantilevered flexible beam with a payload mass attached to the beam free-end. This beam application is then followed by a discussion of a tension and speed setpoint regulating boundary controller for an axially moving web system. Finally, we present a model-based boundary controller that regulates the angular position of a flexible-link robot arm while simultaneously regulating the link vibrations.

16.2 Cantilevered Beam

In many flexible mechanical systems such as flexible link robots, helicopter rotor/blades, space structures, and turbine blades, the flexible element can be modeled as a beam-type structure. The most commonly used beam model that provides a good mathematical representation of the dynamic behavior of the beam is based on the Euler-Bernoulli theory, which is valid when the cross-sectional dimensions of the beam are small in comparison to its length. When deformation owing to shear forces is not inconsequential, a more accurate beam model is provided by the Timoshenko theory, which also incorporates rotary inertial energy. However, owing to its lower order, the Euler-Bernoulli model is often utilized for boundary control design purposes. This section focuses on the problem of stabilizing the displacement of a cantilevered Euler-Bernoulli beam wherein the actuator dynamics at the free-end of the beam have been incorporated into the model. The control law requires shear, shear-rate, and velocity measurements at the free-end of the beam.

16.2.1 System Model

The cantilevered Euler-Bernoulli beam system shown in Figure 16.2 is described by the following PDE:

$$\rho u_{tt}(x,t) + EIu_{xxxx}(x,t) = 0 \tag{16.6}$$

with the following boundary conditions:**

* The detailed mathematical analysis involved in obtaining the final result can be found in Reference 1.

**Given the clamped-end boundary conditions of (16.7), we also know that $u_t(0,t) = u_{xt}(0,t) = 0$.

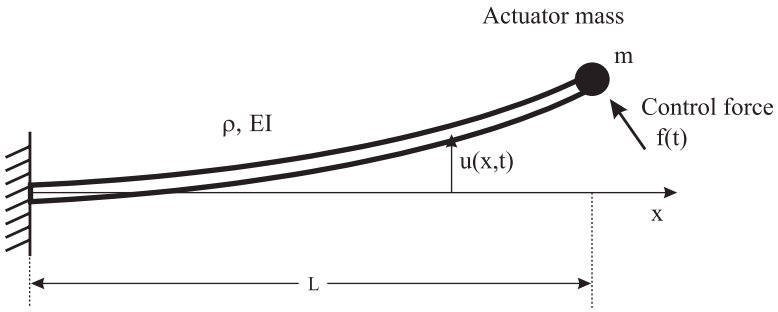

FIGURE 16.2 Schematic diagram of a cantilevered Euler-Bernoulli beam with a free-end payload mass.

$$u(0,t) = u_x(0,t) = u_{xx}(L,t) = 0 \tag{16.7}$$

and

$$mu_{tt}(L,t) - EIu_{xxx}(L,t) = f(t) \tag{16.8}$$

where x,t represent the independent spatial and time variables, the subscripts x,t denote the partial derivatives with respect to x,t, $u(x,t)$ denotes the beam displacement at the position x for time t, ρ is the mass/length of the beam, EI is the bending stiffness of the beam, L is the length of the beam, m represents the payload/actuator mass attached to the free end-point of the beam, and $f(t)$ denotes the boundary control input force.

16.2.2 Model-Based Boundary Control Law

The control objective is to design the boundary control force $f(t)$ that drives the beam displacement $u(x,t)$ to zero with time. Based on the system model, control objectives, and the stability analysis (see Reference 1 or 2 for details), the control force is designed as follows:

$$f(t) = \alpha mu_{xxxt}(L,t) - EIu_{xxx}(L,t) - k_s\eta(t) \tag{16.9}$$

where k_s is a positive control gain and the auxiliary signal $\eta(t)$ is defined as

$$\eta(t) = u_t(L,t) - \alpha u_{xxx}(L,t) \tag{16.10}$$

with α being a positive control gain. A Lyapunov-like analysis,[1] similar to the one given in the motivating example, can be used to show that the system energy (the sum total of the kinetic and potential energy) goes to zero exponentially fast. Standard inequalities can then be invoked to show that $u(x,t)\forall x \in [0,L]$ is bounded by an exponentially decaying envelope; thus, it can easily be established that the beam displacement $u(x,t)$ exponentially decays to zero.

16.2.3 Experimental Trials

A schematic of the experimental setup used in the real-time implementation of the controller is shown in Figure 16.3. A flexible beam 72 cm in length was attached to the top of a support structure with a small metal cylinder weighing 0.3 kg attached to the free end via a strain-gauge shear sensor.

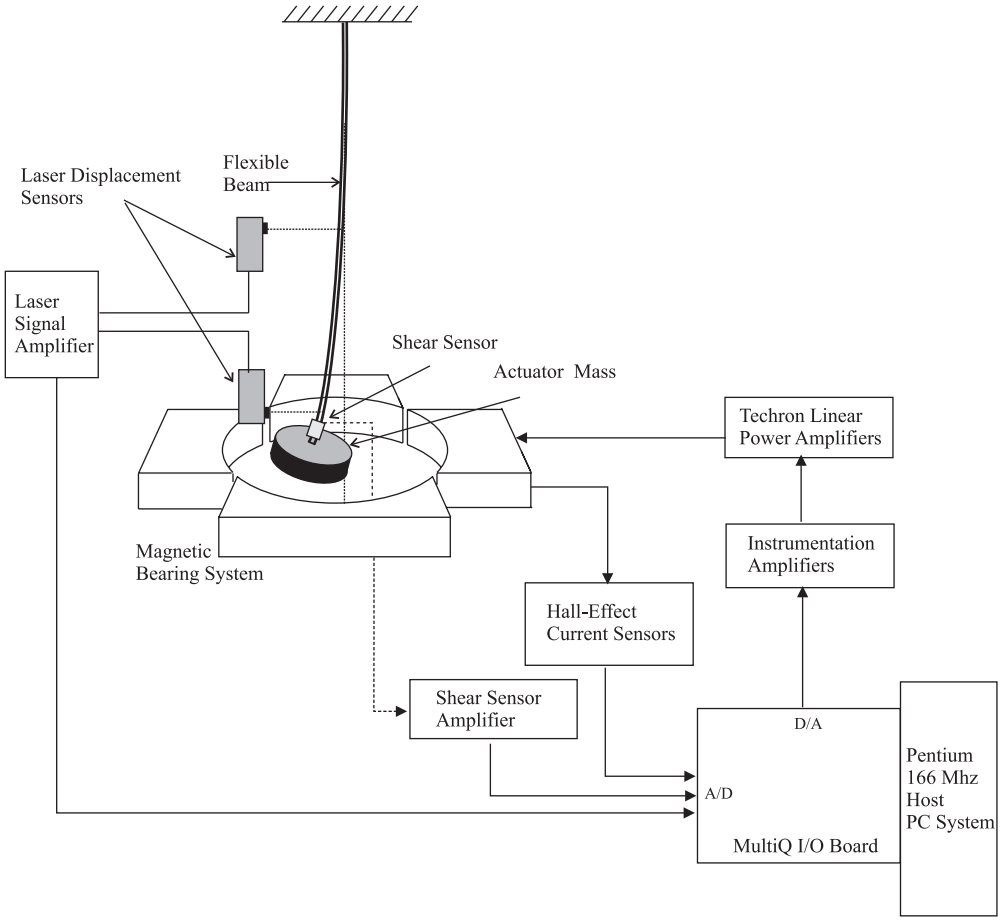

FIGURE 16.3 Schematic diagram of the cantilevered Euler-Bernoulli beam experimental setup.

The beam end-point displacement, $u(L,t)$, was sensed by a laser displacement sensor while another laser displacement sensor was used to monitor the beam mid-point displacement (note that this signal is not used in the control). A pair of electromagnets placed perpendicular to the beam free-end applied the boundary control input force to the payload mass and a custom designed software commutation strategy ensured that the desired input force commanded by the control law was applied to the mass. All time derivatives were calculated using a backwards difference algorithm and a second-order digital filter. The control algorithm was implemented at a 2 kHz sampling frequency on a Pentium 166 MHz PC running QNX (a real-time, micro-kernel-based operating system) under the *Qmotor*[3] graphical user environment.

For this experiment, we imparted an impulse excitation to an arbitrary point on the beam. To ensure a consistent excitation, an impulse hammer was released from a latched position and allowed to strike the beam only once and at the same point each time. The uncontrolled response of the beam's end-point and mid-point displacements when struck by the impulse hammer were recorded.

The response of the model-based boundary controller defined in (16.9) and implemented with three sets of control gains: (i) $k_s = 2.5, \alpha = 1.1$, (ii) $k_s = 5, \alpha = 0.55$, and (iii) $k_s = 7.5, \alpha = 0.38$ is shown in Figure 16.4. It can easily be observed that the model-based controller damps out both the low and high frequency oscillations. For a discussion and comparison of other experiments performed on this system, the reader is referred to Reference 2.

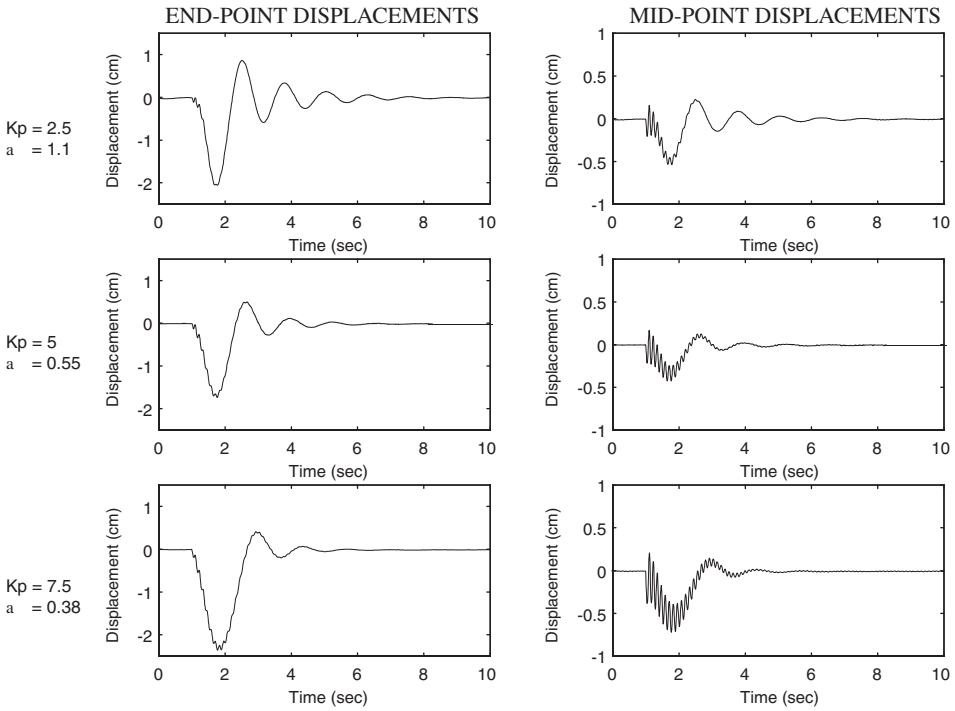

FIGURE 16.4 Cantilevered Euler-Bernoulli beam boundary control response to an impulse excitation.

16.3 Axially Moving Web

In high-speed manufacturing of continuous materials such as optical fibers, textile yarn, paper products, and plastic film, it is imperative to deploy accurate speed and tension control. Typically, rollers are driven to transport these materials through successive operations at varying speeds inherently increasing the risk of controller performance degradation due to tension-varying disturbances. Moreover, tension nonuniformities often lead to product degradation or even failure; hence, precise tension control is essential. Motivated by the need to increase throughput, many manufacturing processes such as those for textile yarn and fibers specify aggressive speed trajectories. Other processes such as label printing demand an aggressive start/stop motion; hence, precise control of such operations relies heavily on coordinated tension and speed control.

16.3.1 System Model

The axially moving web system, depicted in Figure 16.5, consists of a continuous material of length L, axial stiffness EA, and linear density ρ moving between two controlled rollers. Control torques are applied to each roller to regulate the speed of the moving web at a desired setpoint, maintain a constant desired web tension, and damp axial vibration. Based on standard linear web modeling assumptions,[4] the transformed field equation for the axial displacement of the web $u(x,t)$ is given by the following PDE:

$$\rho v_{tt}(x,t) - EAv_{xx}(x,t) = \rho \ddot{y}(t) \tag{16.11}$$

and the boundary conditions

$$v(L,t) = 0 \tag{16.12}$$

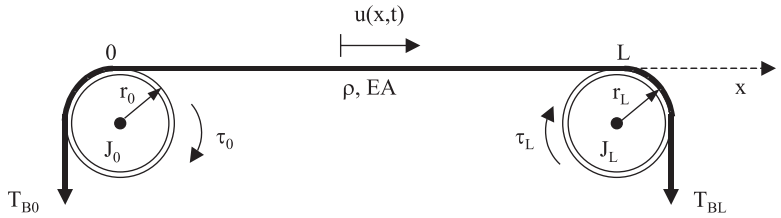

FIGURE 16.5 Schematic diagram of an axially moving web system.

$$mv_{tt}(0,t) - EAv_x(0,t) + P_D = m\ddot{y}(t) - f_0(t) \tag{16.13}$$

where the subscripts denote partial differentiation, the dots over variables denote time differentiation, m is the equivalent mass of the rollers, P_D is the constant desired web tension, and the following transformation* has been used:

$$y(t) = u(L,t) \quad v(x,t) = y(t) - u(x,t) + \frac{P_D}{EA}(x - L). \tag{16.14}$$

While the left roller (at $x = 0$) dynamics are incorporated into (16.13), the right roller dynamics (at $x = L$) are explicitly defined as follows:

$$m\ddot{y}(t) - EAv_x(L,t) + P_D = f_L(t). \tag{16.15}$$

The equivalent force control inputs $f_0(t)$ and $f_L(t)$ in (16.13) and (16.15) are related to the control torques $\tau_0(t)$ and $\tau_L(t)$ as follows:

$$f_0(t) = \frac{\tau_0(t)}{r_0} - T_{B0} \quad f_L(t) = \frac{\tau_L(t)}{r_L} + T_{BL} \tag{16.16}$$

where T_{B0}, T_{BL} denote the web tension in the respective adjacent span and r_0, r_L denote the radii of the rollers.

16.3.2 Model-Based Boundary Control Law

The primary control objective is to design roller torques $\tau_0(t)$ and $\tau_L(t)$ such that the web tension $P(x,t)\forall x \in [0,L]$ is regulated to a constant desired tension setpoint, denoted by P_D, and the web speed $u_t(x,t)\forall x \in [0,L]$ is regulated to a constant desired speed setpoint, denoted by v_d. Based on the system model, control objectives, and the stability analysis,[5] the speed setpoint control law is defined as follows:

$$f_L(t) = P(L,t) + k_p\eta_1(t) + k_i\int_0^t \eta_1(\tau)d\tau \tag{16.17}$$

*The definition of the position/stretch error distribution, denoted by $v(x,t)$, is motivated by the control objective and the stability analysis.

where $P(L,t)$ denotes the web tension at $x = L$, the axial speed setpoint error $\eta_1(t)$ is defined as follows:

$$\eta_1(t) = v_d - \dot{y}(t) = v_d - u_t(L,t)\,, \tag{16.18}$$

v_d denotes the desired web speed setpoint, and k_p, k_i denote constant, positive, scalar gains. The tension setpoint control law is given by

$$f_0(t) = \frac{m\kappa}{EA} P_t(0,t) - P(0,t) + k_{s2}\eta_2(t) + k\eta_1(t) + k_i \int_0^t \eta_1(\tau)d\tau \tag{16.19}$$

where the tension setpoint error $\eta_2(t)$ is defined as

$$\eta_2(t) = v_t(0,t) - \kappa v_x(0,t) = u_t(L,t) - u_t(0,t) - \frac{\kappa}{EA}\left(P_D - P(0,t)\right), \tag{16.20}$$

$P(0,t)$ denotes the tension at $x = 0$, $P_t(0,t)$ denotes the rate change in tension at $x = 0$, and κ, k_{s2} denote positive scalar control gains. After using a Lyapunov-like analysis,[5] similar to one given in the motivating example, it can be shown that $v_t(x,t)$ and $v_x(x,t)$ exponentially decay to zero. Thus, the time derivative of (16.14) yields velocity setpoint regulation (i.e., $u_t(x,t)$ is exponentially driven to v_d). Furthermore, given that the web tension is related to the axial strain as follows: $P(x,t) = EAu_x(x,t)$, the spatial derivative of (16.14) yields tension setpoint regulation (i.e., $EAu_x(x,t)$ is exponentially driven to P_D). For more details, the reader is referred to Ulsoy.[5]

16.3.3 Experimental Trials

The experimental test stand consisted of an elastic rubber belt moving axially over two pulleys actuated by brushed DC motors (see Figure 16.6). Four tension sensors and roller assemblies laterally positioned the moving web and provided measurements of the forward boundary tensions $P(0,t)$ and $P(L,t)$ and the back boundary tensions T_{B0} and T_{BL} used by the controller. The encoders mounted on the motors measured the angular displacements of the rotors. The control algorithm was implemented with a sampling period of 0.5 msec on a Pentium 266 MHz PC running QNX OS under the *Qmotor* graphical user environment.[3]

The objective of the experiment was to regulate the material tension at 8.0 N and move the material according to a smooth, exponentially stepped, desired axial speed setpoint trajectory. In order to mimic real-world industrial processes (such as high-speed label printing), the desired speed of the material was aggressively driven to 0 m/s and back to 0.75 m/s within a time duration of 0.5 sec and was repeated every 10 sec. Process-line disturbances leading to a sudden change in material tension were also simulated by applying a constant reverse torque on the motor at $x = 0$ for a duration of 0.5 sec at 10 sec intervals. Figure 16.7 shows the boundary controller performance.

From the experimental results,[5] it was observed that the maximum speed error at $x = 0$ with the boundary controller was three times smaller than industry standard controllers. With a start-stop speed disturbance, the boundary controller improved tension setpoint regulation by a factor of three over a PI speed controller without tension feedback and a factor of two over a PI speed controller with tension feedback.

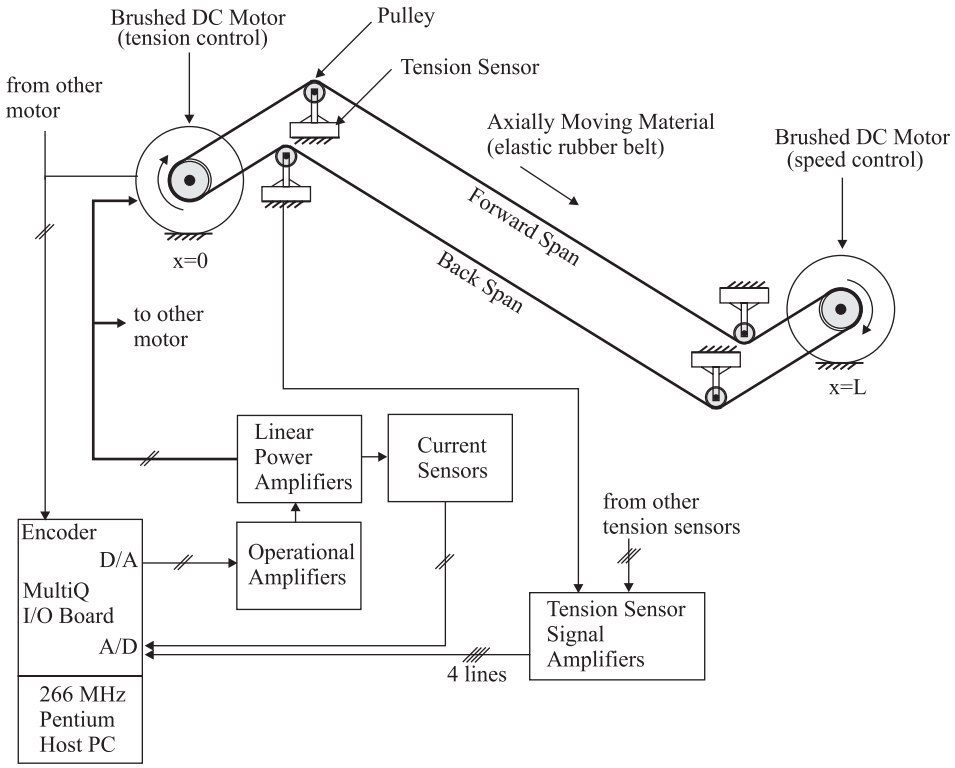

FIGURE 16.6 Schematic diagram of the axially moving web experimental setup.

16.4 Flexible Link Robot Arm

Owing to the prohibitive cost of placing heavy equipment in outer space, most structural designers prefer to utilize lightweight materials in the construction of space-based vehicles, satellites, etc. Indeed, space-based robot manipulators are more likely to be comprised of long links manufactured from lightweight metals or composites. Unfortunately, a major drawback in using lightweight links is the significant presence of deflection and/or vibration problems during position control applications. In this section, we focus our attention on regulating the angular displacement of a flexible link robot manipulator arm described by a nonlinear PDE model while simultaneously reducing the distributed vibration of the link itself.

16.4.1 System Model

The robot system, illustrated in Figure 16.8, is composed of an Euler-Bernoulli beam clamped to a rotating, rigid actuator hub with a payload/actuator mass attached to the free end of the beam. A torque input applied to the hub controls the angular position while a force input that is applied to the free-end mass regulates the beam displacement. The equations of motion of this single flexible-link robot are given by[6]

$$\rho w_{tt}(x,t) + EIw_{xxxx}(x,t) = \rho u(x,t)\dot{q}^2(t) \tag{16.21}$$

and

$$D(t)\ddot{q}(t) + \tfrac{1}{2}\dot{D}(t)\dot{q}(t) + V_m(t)\dot{q}(t) + mu(L,t)w_t(L,t)\dot{q}(t) - EIw_{xx}(0,t) = \tau(t) \tag{16.22}$$

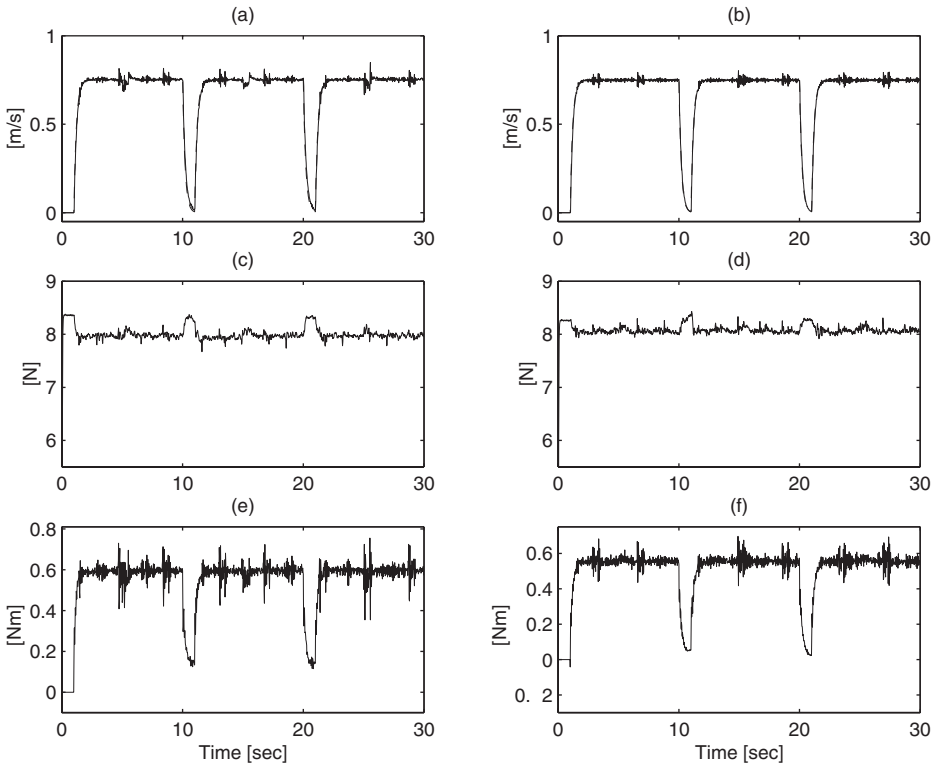

FIGURE 16.7 Axially moving web system control response.

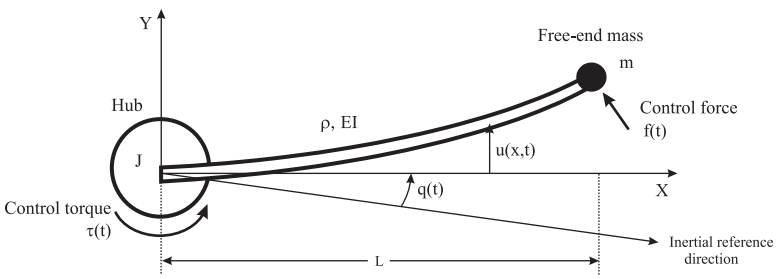

FIGURE 16.8 Schematic diagram of the flexible-link robot arm.

with the following boundary conditions:*

$$u(0,t) = u_x(0,t) = u_{xx}(L,t) = 0 \tag{16.23}$$

and

$$mw_{tt}(L,t) - mu(L,t)\dot{q}^2(t) - EIw_{xxx}(L,t) = f(t) \tag{16.24}$$

*Given the clamped boundary conditions of (16.23), we also know that $u_t(0,t) = u_{xt}(0,t) = 0$.

where the distributed displacement $w(x,t)$ is defined as

$$w(x,t) = u(x,t) + xq(t) \tag{16.25}$$

and $u(x,t)$ denotes the link displacement at position x for time t with respect to the (X, Y) coordinate system that rotates with the hub (see Figure 16.8), $q(t), \dot{q}(t), \ddot{q}(t)$ represent the angular position, velocity, and acceleration of the hub, respectively, with respect to the inertial reference direction, ρ is the mass/length of the link, EI is the bending stiffness of the link, L is the length of the link, m represents a payload/actuator mass attached to the free end of the link, $\tau(t)$ is the control torque input applied to the hub, $f(t)$ denotes the boundary control force input applied to the mass, and the auxiliary functions $D(t), D(t)$, and $V_m(t)$ are defined as follows:

$$D(t) = J + mu^2(L,t) + \rho \int_0^L u^2(\sigma,t)d\sigma \geq J > 0 \tag{16.26}$$

$$\dot{D}(t) = \tfrac{d}{dt} D(t) = 2mu(L,t)u_t(L,t) + 2\rho \int_0^L u(\sigma,t)u_t(\sigma,t)d\sigma \tag{16.27}$$

and

$$V_m(t) = \rho \int_0^L u(\sigma,t)w_t(\sigma,t)d\sigma \tag{16.28}$$

with J denoting the hub's inertia.

16.4.2 Model-Based Boundary Control Law

The control objective is to ensure that: (i) $u(x,t) \to 0 \forall x \in [0,L]$ as $t \to \infty$ with respect to the rotating coordinate system (X, Y) attached to the hub, and (ii) $q(t) \to q_d$ as $t \to \infty$ with respect to the inertial reference direction, where q_d is a desired, constant angular position. To aid the analysis of the link displacement regulation objective, an auxiliary signal $\eta(t)$, is defined as follows:

$$\eta(t) = w_t(L,t) - w_{xxx}(L,t) \tag{16.29}$$

where $w(x,t)$ was defined in (16.25). The angular position regulation objective is quantified via the angular position setpoint error $e(t)$ as follows:

$$e(t) = q(t) - q_d \,. \tag{16.30}$$

Based on the form of (16.29), the stability analysis, and the control objective, the boundary control force is designed as follows:

$$f(t) = mw_{xxxt}(L,t) - EIw_{xxx}(L,t) - k_s\eta(t) \tag{16.31}$$

where k_s is a positive control gain. Similarly, the hub control torque is designed as follows:

$$\tau(t) = -k_v\dot{e}(t) - k_p e(t) + mu(L,t)\dot{q}(t)w_{xxx}(L,t) - \beta\rho L\dot{q}(t)u^2(L,t) \tag{16.32}$$

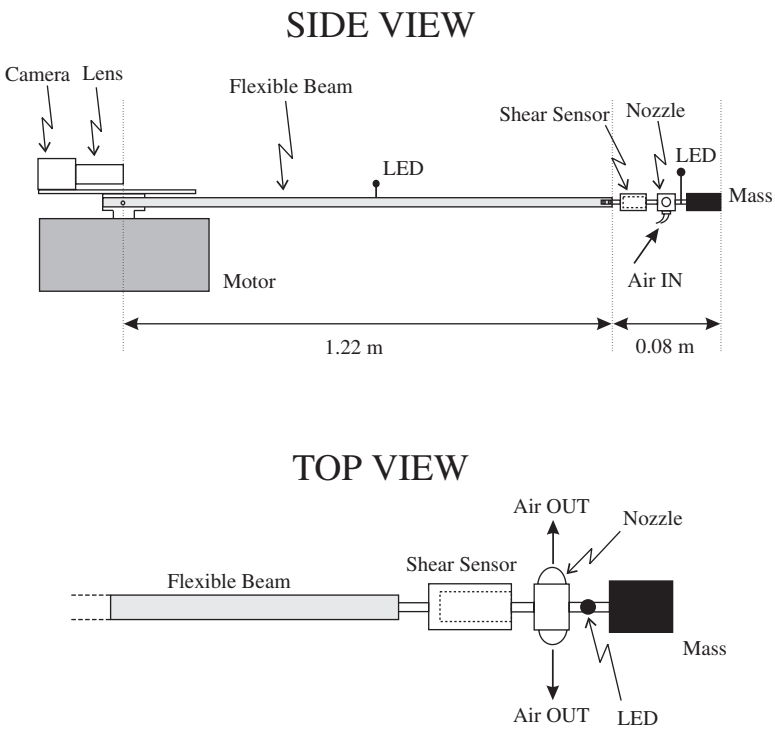

FIGURE 16.9 Schematic diagram of the flexible-link robot arm experimental setup.

where k_v, k_p, β are positive control gains. A Lyapunov-like analysis,[1] similar to one given in the motivating example, can be used to show that the system energy (the sum total of the kinetic and potential energy) asymptotically goes to zero. Standard inequalities can then be invoked to show that the beam displacement $w(x,t) \forall x \in [0, L]$ and the angular position setpoint error $e(t)$ are both asymptotically driven to zero. It is also interesting to note that the boundary control force of (16.31) contains a noncollocated term in the feedback loop (i.e., $\dot{q}(t)$ appears in the definition of $\eta(t)$ through $w_t(L,t)$) while the control torque of (16.32) contains noncollocated feedforward and feedback terms (i.e., the last two terms in (16.32)).

16.4.3 Experimental Trials

A schematic diagram of the experimental setup shown in Figure 16.9 consisted of a flexible aluminum beam attached to the shaft of a switched reluctance motor (SRM) that was used to apply the hub control torque. A lightweight plastic assembly supporting two air nozzles located at the end-point of the beam was used to apply the boundary control force with a 90 psi compressed air supply to high-speed proportional air valves. In addition, a modular line scan camera mounted on the motor shaft and a high luminescence LED mounted at the beam's end-point were used to measure the beam's end-point displacement, $u(L,t)$. A second monitoring LED was placed at $u(L/2,t)$. The signal $u_{xxx}(L,t)$ was measured via the shear force sensor attached to the beam free-end, while an incremental encoder mounted on the motor shaft was utilized to measure the hub angular position, $q(t)$. All time derivatives were calculated using a backwards difference algorithm and a second-order digital filter. The controller was implemented via the *Qmotor* real-time control environment[3] on a QNX platform using a sampling period of 0.5 msec.

The objective of the experiment was to regulate the hub angular position to a desired position of 20° (i.e., $q_d = 0.35$ rad) while driving the link displacement to zero. For comparison purposes,

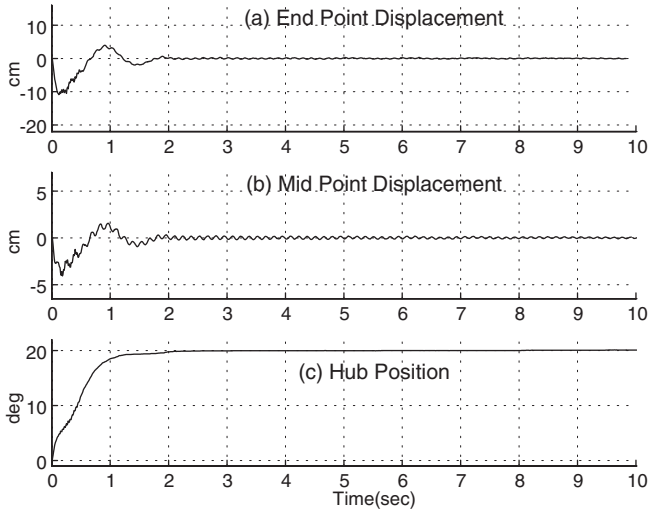

FIGURE 16.10 Flexible-link robot arm boundary control response.

a standard linear control algorithm along the hub angular setpoint error and with the air valves deactivated was implemented. The model-based boundary controller was implemented with $k_s = 3.5, k_v = 20, k_p = 70$, and $\beta = 0.35$ (see Figure 16.10). From the experimental results,[7] it was observed that while the standard linear control law did not damp out beam vibrations even after 10 sec, the model-based boundary controller was able to regulate the distributed beam vibrations within approximately 3 sec as can be seen in Figure 16.10.

16.5 Summary

A number of researchers have investigated vibration control for flexible mechanical systems. For example, Ulsoy[8] demonstrated how control and observation spillover can destabilize[9] the vibration of an axially moving string under state feedback control based on a reduced-order, discretized version of the infinite dimensional model. While Yang and Mote[10] used a transfer function approach to develop asymptotically stabilizing controllers to avoid spillover instabilities, Lee and Mote[11] developed Lyapunov-based, boundary control laws that asymptotically stabilized the vibration of an axially moving string. Other researchers such as Morgul,[12] Shahruz,[13] Joshi and Rahn,[14] and Baicu et al.[15] have designed boundary controllers for strings, overhead gantry crane systems, and flexible cable systems. More recently, Zhang et al.[16] and Nagarkatti et al.[17] designed boundary controllers for nonlinear string models and axially accelerating web systems, respectively.

For cantilevered beams, boundary controllers have been proposed by Morgul,[18,19] Chen et al.[20] Canbolat et al.,[2] and Rahn and Mote,[21] whereas boundary controllers for single flexible link robots were developed by Luo et al.[22-25] and Morgul.[26] Recently, Queiroz et al.[7] designed a boundary control strategy for a nonlinear hybrid model of flexible link robots that asymptotically regulated the link displacement and hub position.

In this chapter, we focused our attention on boundary controllers that regulated vibration for a class of mechanical systems described by second-order (in time) PDE models. It should be noted that the boundary control philosophy has also been applied to other kinds of systems. For example, Byrnes,[27] Krstic,[28] and van Ly[29] designed boundary controllers for the Burgers' equation, which serves as a model for a number of physical problems and is representative of many convection-dominated flow systems. Boundary controllers (e.g., Reference 30) have also been designed for the Kuramoto-Sivashinsky equation that is used to describe a variety of systems such as a plane flame front, flow of thin liquid films on inclined planes, and Alfven drift wave plasmas.

Acknowledgments

The authors wish to thank Bret Costic, Marcio de Queiroz, and Erkan Zergeroglu for their assistance in the formatting of this chapter.

References

1. M. S. de Queiroz, D. M. Dawson, S. P. Nagarkatti, and F. Zhang, *Lyapunov-Based Control of Mechanical Systems*, Birkhauser, Basel, Switzerland, 1999.
2. H. Canbolat, D. Dawson, C. Rahn, and P. Vedagarbha, Boundary control of a cantilevered flexible beam with point-mass dynamics at the free end, *Mechatronics — An International Journal,* 8, 3, 163–186.
3. N. Costescu, D. M. Dawson, and M. Loffler, Qmotor 2.0 — a PC based real-time multitasking graphical control environment, *IEEE Control Systems Magazine Applications*, 18, 1, 13–22, 1999.
4. J. Wickert and C. D. Mote, Jr., Current research on the vibration and stability of axially-moving materials, *Shock and Vibration Digest*, 20, 5, 3–13, 1988.
5. S. P. Nagarkatti, F. Zhang, C. D. Rahn, and D. M. Dawson, Tension and speed setpoint regulation for axially moving materials, *ASME Journal of Dynamic Systems, Measurement, and Control,* 122, 3, 445–453, 2000.
6. J. L. Junkins and Y. Kim, *Introduction to Dynamics and Control of Flexible Structures*, AIAA Education Series, Washington, D.C., 1993.
7. M. S. de Queiroz, D. M. Dawson, M. Agarwal, and F. Zhang, Adaptive nonlinear boundary control of a flexible link robot arm, *IEEE Transactions on Robotics and Automation,* 15, 4, 779–787, 1999.
8. A. G. Ulsoy, Vibration control in rotating or translating elastic systems, *ASME Journal of Dynamic Systems, Measurement, and Control*, 106, 1, 6–14, 1984.
9. M. Balas, Active control of flexible systems, *Journal of Optimization Theory and Applications*, 25, 3, 415–436, 1978.
10. B. Yang and C. D. Mote, Jr., Active vibration control of the axially moving string in the S domain, *ASME Journal of Applied Mechanics*, 58, 189–196, 1991.
11. S. Y. Lee and C. D. Mote, Jr., Vibration control of an axially moving string by boundary control, *ASME Journal of Dynamic Systems, Measurement, and Control*, 118, 66–74, 1996.
12. O. Morgul, A dynamic control law for the wave equation, *Automatica*, 30, 11, 1785–1792, 1994.
13. S. M. Shahruz and L. G. Krishna, Boundary control of a nonlinear string, *Proceedings of the ASME Dynamics Systems and Control Division*, DSC-58, 831–835, 1996.
14. S. Joshi and C. D. Rahn, Position control of a flexible cable gantry crane: theory and experiment, *Proceedings of the American Control Conference*, Seattle, 2820–2824, 1995.
15. C. F. Baicu, C. D. Rahn, and B. D. Nibali, Active boundary control of elastic cables: Theory and experiment, *Journal of Sound and Vibration*, 198, 1, 17–26, 1996.
16. F. Zhang, D. M. Dawson, S. P. Nagarkatti, and C. D. Rahn, Boundary control for a general class of nonlinear actuator-string systems, *Journal of Sound and Vibration*, 229, 1, 113–132, 2000.
17. S. P. Nagarkatti, F. Zhang, B. T. Costic, D. M. Dawson, and C. D. Rahn, Velocity tracking control of an axially accelerating web and actuator system, *Mechanical Systems and Signal Processing*, accepted 2001 (to appear).
18. O. Morgul, Orientation and stabilization of a flexible beam attached to a rigid body: Planar motion, *IEEE Transactions on Automatic Control*, 36, 8, 953–962, 1991.
19. O. Morgul, Dynamic boundary control of a Euler-Bernoulli beam, *IEEE Transactions on Automatic Control*, 37, 5, 639–642, 1992.
20. G. Chen, M. Delfour, A. Krall, and G. Payre, Modeling, stabilization, and control of serially connected beams, *SIAM Journal of Control Optimizations*, 25, 3, 526–546, 1987.
21. C. Rahn and C. Mote, Axial force stabilization of transverse beam vibration, *Proceedings of the ASME Conference on Mechanical Vibration and Noise*, Albuquerque, DE-61, 29–34, 1993.
22. Z. Luo, Direct strain feedback control of flexible robot arms: New theoretical and experimental results, *IEEE Transactions on Automatic Control*, 38, 11, 1610–1622, 1993.

23. Z. Luo and B. Guo, Further theoretical results on direct strain feedback control of flexible robot arms, *IEEE Transactions on Automatic Control,* 40, 4, 747–751, 1995.
24. Z. Luo, N. Kitamura, and B. Guo, Shear force feedback control of flexible robot arms, *IEEE Transactions on Robotics and Automation,* 11, 5, 760–765, 1995.
25. Z. H. Luo and B. Z. Guo, Shear force feedback control of a single-link flexible robot with a revolute joint, *IEEE Transactions on Automatic Control*, 42, 1, 53–65, 1997.
26. O. Morgul, On boundary control of single link flexible robot arms, *IFAC World Congress*, San Francisco, A, 127–132, 1996.
27. C. I. Byrnes, D. S. Gilliam, and V. I. Shubov, Boundary control for a viscous Burgers' equation, *Identification and Control for Systems Governed by Partial Differential Equations*, SIMA, 171–185, 1993.
28. M. Krstic, On global stabilization of Burgers' equation by boundary control, *Systems and Control Letters*, 37, 123–142, 1999.
29. H. van Ly, K. D. Mease, and E. S. Titi, Distributed and boundary control of the viscous Burgers' equation, *Numerical Function Analysis and Optimization*, 18, 143–188, 1997.
30. W. J. Liu and M. Krstic, Stability enhancement by boundary control in the Kuramoto-Sivashinsky equation, *Nonlinear Analysis*, 1999.